



Empirical proton-neutron interaction of even Ra isotopes probed by the quadrupole-octupole collective Hamiltonian based on the covariant density functional

W. Zhang (张炜)¹ and S. Q. Zhang (张双全)^{2,*}

¹*School of Physics and Microelectronics, Zhengzhou University, Zhengzhou 450001, China*

²*State Key Laboratory of Nuclear Physics and Technology, School of Physics, Peking University, Beijing 100871, China*



(Received 24 July 2019; revised manuscript received 25 September 2019; published 4 November 2019)

The empirical proton-neutron interaction δV_{pn} for even-even Ra isotopes is analyzed by using the covariant density functional theory and the quadrupole-octupole collective Hamiltonian approach. It is shown that the static deformation and collective fluctuation are crucial ingredients for good reproduction of the data. Particularly, the introduction of octupole deformation β_3 dramatically changes the δV_{pn} with $N = 134, 136, 140$. The collective fluctuation smoothly corrects the δV_{pn} with good trend. Taking ^{224}Ra as an example, the detailed contributions from the static deformation and the collective fluctuation are analyzed, and the microscopic single-particle levels, the octupole driving pairs, and the enhancement of proton-neutron interaction are discussed.

DOI: [10.1103/PhysRevC.100.054303](https://doi.org/10.1103/PhysRevC.100.054303)

I. INTRODUCTION

For an atomic nucleus, the average proton-neutron (p-n) interaction of the last nucleons, δV_{pn} , may be empirically extracted from a specific double difference of the binding energies [1,2], for instance for an even-even isotope (Z, N) , $\delta V_{pn} = -1/4[E(Z, N) - E(Z, N - 2) - E(Z - 2, N) + E(Z - 2, N - 2)]$. The strengths of δV_{pn} are suggested to reflect a wealth of nuclear structural properties including shell closure, Wigner energy, the onset and development of collectivity, and shape transitions [3–7], and therefore have attracted a great deal of empirical analysis [8–15] and microscopic studies [7,16–19]. For a recent review, see Ref. [20]. In addition, with the help of the systematics of δV_{pn} , it is useful to propose local mass relations to describe experimental data of nuclear masses and to predict some of the unknown masses [21].

Particularly in the region of Ra isotopes, the fine structure of δV_{pn} has drawn a focused attention [19,22–24]. In 2006, it was noted that there are anomalies of δV_{pn} for $^{221,223}\text{Ra}$ with $N = 133, 135$ deviating from the general trend, i.e., the so-called Ra puzzle [22]. Later, with a precise Penning-trap mass measurement on $^{223-229}\text{Rn}$, the existence of Ra puzzle was confirmed [23]. A well-developed peak around $N = 135$, which terminates at $N = 139$, is clearly shown for δV_{pn} of the odd- A Ra isotopes.

Microscopically, it is speculated that the Ra puzzle is associated with the softness of well-known octupole deformation in this region around $Z = 88$ and $N = 134$ [22,23]. For this region, the octupole correlation is associated with the interaction between the orbital pairs with $\Delta l = 3$ and $\Delta j = 3$ of neutron ($\nu 2g_{9/2}$, $\nu 1j_{15/2}$) and also of proton ($\pi 2f_{7/2}$, $\pi 1i_{13/2}$) around the Fermi surfaces [25].

Starting from microscopic density functional theories [26–30], attempts for understanding Ra puzzle have been carried out [19,24]. In Ref. [24], a reflection asymmetric covariant density functional theory (CDFT) was employed. The octupole deformation and shape evolution in the Ra and Rn isotopes were examined in the potential energy surfaces (PESs) of (β_2, β_3) plane, and the strengths of δV_{pn} for Ra isotopes extracted from the reflection asymmetric CDFT calculations were compared with the data as well as the axial and the triaxial calculations. It was found that the octupole deformation does play a significant role in the Ra puzzle [24]. In Ref. [19], δV_{pn} for Ra and Th isotopes were discussed with the framework of the deformed Hartree-Fock-Bogoliubov (HFB) with Gogny interaction as well as the generator coordinate method (GCM) to deal with the beyond-mean-field effects [31,32]. Good agreement with the experimental δV_{pn} for the even Ra isotopes with $N = 134$ – 142 was obtained there whereas a large discrepancy was shown for a lighter isotope with $N = 132$. The impact of quadrupole-octupole coupling correlations on the behavior of δV_{pn} is found to be small but it always goes in the direction of improving the agreement with experiment [19].

Similar to Ref. [19], on top of the framework of CDFT instead, it is interesting to probe the collective correlations on the δV_{pn} for the even Ra isotopes. As it is known, the CDFT has been exploited in describing ground-state properties of both spherical and deformed nuclei all over the nuclear chart [26,28–30], including superheavy nuclei [33], hypernuclei [34–36], and thermal nuclei [37,38]. In particular, there is a very successful relativistic density functional PC-PK1 [39] turned out to provide good descriptions for the isospin dependence of the binding energy along either the isotopic or the isotonic chain [40]. After taking into account dynamic correlation energies, the root-mean-square (rms) deviation with respect to nuclear masses of 575 even-even nuclei has been reduced to 1.14 MeV, superior to other successful density

*sqzhang@pku.edu.cn

functionals [41]. Very recently, to further consider collective fluctuations in reflection asymmetric degrees of freedom, the quadrupole-octupole collective Hamiltonian (QOCH) on top of the covariant density functional has been developed [42–45].

Therefore, the present paper will be devoted to the empirical proton-neutron interaction of even Ra isotopes by the successive use of the CDFT and QOCH methods. The fine structure of the δV_{pn} for the even Ra isotopes will be analyzed in detail on the mean-field level and the beyond-mean-field level. The important roles of the octupole deformation and the collective correlations will be addressed. We also analyze the detailed components of single-particle levels as well as the contributions from the octupole driving pairs.

II. THEORETICAL FRAMEWORK

In this section, the theoretical framework of CDFT and QOCH will be briefly introduced. The detailed formalism of the CDFT can be found in Refs. [39,46,47], and the details of the QOCH method can be found in Refs. [43,44].

The starting point of the point-coupling CDFT is an effective Lagrangian density with zero-range interaction between nucleons:

$$\begin{aligned} \mathcal{L} = & \bar{\psi}(i\gamma_\mu \partial^\mu - m)\psi \\ & - \frac{1}{2}\alpha_S(\bar{\psi}\psi)(\bar{\psi}\psi) - \frac{1}{2}\alpha_V(\bar{\psi}\gamma_\mu\psi)(\bar{\psi}\gamma^\mu\psi) \\ & - \frac{1}{2}\alpha_{TV}(\bar{\psi}\vec{\tau}\gamma_\mu\psi) \cdot (\bar{\psi}\vec{\tau}\gamma^\mu\psi) \\ & - \frac{1}{3}\beta_S(\bar{\psi}\psi)^3 - \frac{1}{4}\gamma_S(\bar{\psi}\psi)^4 - \frac{1}{4}\gamma_V[(\bar{\psi}\gamma_\mu\psi)(\bar{\psi}\gamma^\mu\psi)]^2 \\ & - \frac{1}{2}\delta_S\partial_\nu(\bar{\psi}\psi)\partial^\nu(\bar{\psi}\psi) - \frac{1}{2}\delta_V\partial_\nu(\bar{\psi}\gamma_\mu\psi)\partial^\nu(\bar{\psi}\gamma^\mu\psi) \\ & - \frac{1}{2}\delta_{TV}\partial_\nu(\bar{\psi}\vec{\tau}\gamma_\mu\psi) \cdot \partial^\nu(\bar{\psi}\vec{\tau}\gamma^\mu\psi) \\ & - \frac{1}{4}F^{\mu\nu}F_{\mu\nu} - e\bar{\psi}\gamma^\mu\frac{1-\tau_3}{2}\psi A_\mu, \end{aligned} \quad (1)$$

which includes the free nucleon term, the four-fermion point-coupling terms, the higher-order terms, which are responsible for the effects of medium dependence, the gradient terms, which are included to simulate the effects of finite range, and the electromagnetic interaction terms. The Dirac spinor field of the nucleon is denoted by ψ , and the nucleon mass is m . α , β , γ , and δ with subscripts S (scalar), V (vector), TV (isovector) are coupling constants (adjustable parameters) in which α refers to the four-fermion term, β and γ , respectively, to the third- and fourth-order terms, and δ the derivative couplings.

By means of the conventional variation principle, the Dirac equation for nucleons can be obtained

$$[\gamma_\mu(i\partial^\mu - V^\mu) - (m + S)]\psi_k = 0, \quad (2)$$

where $\psi_k(\mathbf{r})$ denotes the Dirac spinor field of a nucleon. The scalar $S(\mathbf{r})$ and vector potential $V^\mu(\mathbf{r})$ are calculated in terms of the isoscalar density, isoscalar current, and isovector current. These densities and currents are calculated using

$\psi_k(\mathbf{r})$. Thus one can use iteration to obtain the self-consistent solutions.

The total binding energies E_{tot} at different axial-symmetric shapes (β_2, β_3) can be obtained by applying constraints with quadrupole deformation β_2 and octupole deformation β_3 simultaneously. In the mean-field level, the binding energy at a given deformation (β_2, β_3) can be obtained by minimizing

$$\langle H' \rangle = \langle H \rangle + \frac{1}{2}C_2(\langle \hat{Q}_2 \rangle - \mu_2)^2 + \frac{1}{2}C_3(\langle \hat{Q}_3 \rangle - \mu_3)^2, \quad (3)$$

where C_2 and C_3 are two spring constants, $\langle \hat{Q} \rangle$ is the expectation value of moment operator where the quadrupole and octupole moment operators read $\hat{Q}_2 = 2r^2P_2(\cos\theta)$ and $\hat{Q}_3 = 2r^3P_3(\cos\theta)$, respectively, and μ_2 and μ_3 are given quadrupole and octupole moments, which are related to the quadrupole and octupole deformations by $\mu_2 = \frac{3AR^2}{4\pi}\beta_2$ and $\mu_3 = \frac{3AR^3}{4\pi}\beta_3$, respectively. Based on the total binding energies E_{tot} at the mesh points in the (β_2, β_3) plane, the global minimum state with the lowest energy $E_{\text{min}}(\beta_2, \beta_3)$ is obtained. The deformation energies are calculated as the energy differences between states with certain deformation or restrictions.

The collective Hamiltonian method is a simplified generator coordinate method by exploiting the Gaussian overlap approximation (GOA) [48]. In the GCM, one can build approximate eigenstates of the nuclear Hamiltonian starting from a set of mean-field states that depend on a collective coordinate q . This leads to the Hill-Wheeler-Griffin (HWG) integral equation. With the assumption that the overlap kernels can be approximated by Gaussian functions, the local expansion of the kernels up to second order in the nonlocality transforms the HWG equation into a second-order differential equation—the Schrödinger equation for the collective Hamiltonian

$$\hat{H}_{\text{coll}}g_\alpha(q) = E_\alpha g_\alpha(q), \quad (4)$$

where q donates the continuous collective variables. By solving this equivalent eigenvalue problem, the properties of low-lying states especially the state with the lowest energy $E(0^+)$ considering the collective fluctuation are obtained.

In the quadrupole-octupole collective Hamiltonian method [43], q in Eq. (4) stands for the quadrupole and octupole deformation β_2, β_3 , and the Euler angle Ω . In details, the collective Hamiltonian is composed of the vibrational kinetic energy \hat{T}_{vib} , the rotational kinetic energy \hat{T}_{rot} and the collective potential V_{coll} :

$$\hat{H}_{\text{coll}} = \hat{T}_{\text{vib}} + \hat{T}_{\text{rot}} + V_{\text{coll}}. \quad (5)$$

The vibrational and rotational kinetic energies are

$$\begin{aligned} \hat{T}_{\text{vib}} = & -\frac{\hbar^2}{2\sqrt{w\mathcal{I}}} \left[\frac{\partial}{\partial\beta_2} \sqrt{\frac{\mathcal{I}}{w}} B_{33} \frac{\partial}{\partial\beta_2} - \frac{\partial}{\partial\beta_2} \sqrt{\frac{\mathcal{I}}{w}} B_{23} \frac{\partial}{\partial\beta_3} \right. \\ & \left. - \frac{\partial}{\partial\beta_3} \sqrt{\frac{\mathcal{I}}{w}} B_{23} \frac{\partial}{\partial\beta_2} + \frac{\partial}{\partial\beta_3} \sqrt{\frac{\mathcal{I}}{w}} B_{22} \frac{\partial}{\partial\beta_3} \right], \end{aligned} \quad (6)$$

$$\hat{T}_{\text{rot}} = \frac{\hat{J}^2}{2\mathcal{I}}, \quad (7)$$

where the mass parameters B_{22}, B_{23} , and B_{33} and the moment of inertia \mathcal{I} are functions of the quadrupole β_2 and octupole β_3

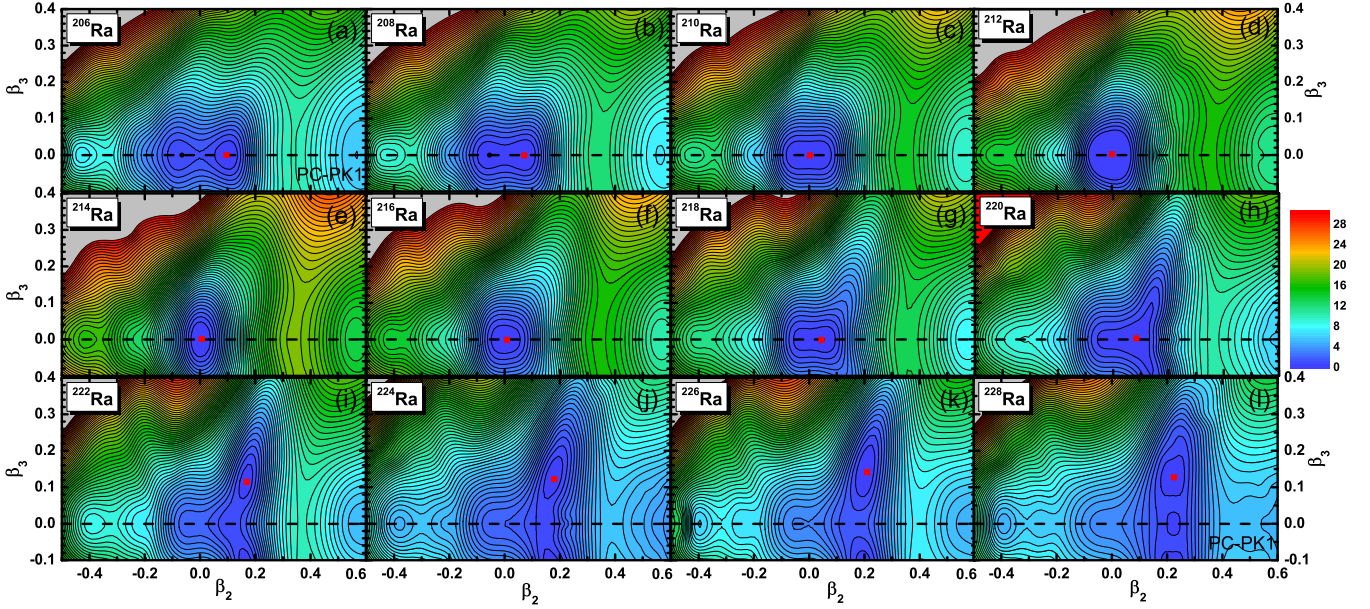


FIG. 1. The contour plots of total energies for even-even isotopes $^{206-228}\text{Ra}$ in (β_2, β_3) plane obtained in CDFT with effective interaction PC-PK1. The energy separation between contour lines is 0.5 MeV. The global minima are denoted by the square.

deformations, $w = B_{22}B_{33} - B_{23}^2$, and \hat{J} denotes the angular momentum perpendicular to the intrinsic symmetric axis. The mass parameters B_{22} , B_{23} , and B_{33} are further calculated in the perturbative cranking approximation [49], while the moment of inertia \mathcal{I} is calculated according to the Inglis-Belyaev formula [50,51].

The collective potential V_{coll} is obtained by subtracting the zero-point energy (ZPE) from the total binding energy E_{tot} . The ZPE corrections has vibrational and rotational parts, which are calculated in the cranking approximation [49,52],

$$\Delta V_{\text{vib}} = \frac{1}{4} \text{Tr}[\mathcal{M}_{(3)}^{-1} \mathcal{M}_{(2)}], \quad (8)$$

$$\Delta V_{\text{rot}} = \frac{\langle \hat{J}^2 \rangle}{2\mathcal{I}}, \quad (9)$$

where \mathcal{M} is energy-weighted moment tensor.

The collective parameters used in the Hamiltonian [Eq. (5)], like the mass parameters, are determined in the CDFT calculation microscopically. The eigenvalue problem of the collective Hamiltonian Eq. (4) is solved by expanding the eigenfunctions in terms of a complete set of basis functions.

III. RESULTS AND DISCUSSION

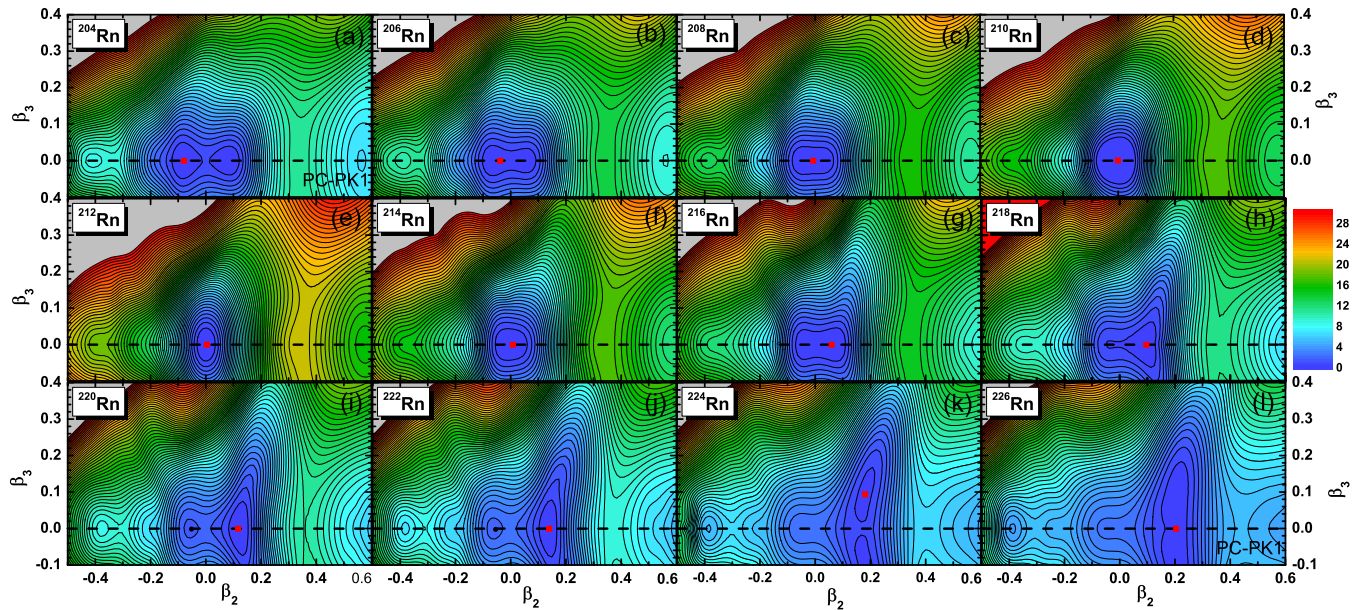
Within the framework of covariant density functional theory, the residual proton-neutron interactions δV_{pn} in Ra isotopes have been investigated with the reflection asymmetric relativistic mean-field (RAS-RMF) theory as well as the triaxial CDFT calculations in Ref. [24], where the pairing correlations are neglected. It was found that the octupole deformation is responsible for the fine structure of δV_{pn} in Ra isotopes, which is called Ra puzzle, whereas the inclusion of triaxiality changes little on their absolute values. Thus in the

present paper, which intends to examine the beyond-mean-field effect on δV_{pn} by collective Hamiltonian, we will limit the study within the axial quadrupole and octupole degrees of freedom.

In the CDFT calculations, one of the most successful covariant density functionals with the point-coupling form, PC-PK1 [39] is employed. Pairing correlations are taken into account by the standard BCS method with a smooth cutoff factor to simulate the effect of finite range [53,54]. A density-independent δ force in the pairing channel is adopted and its pairing strength for neutron (proton) is -349.5 (-330.0) MeV fm³ for density functional PC-PK1 [39].

To obtain the collective parameters in the quadrupole-octupole collective Hamiltonian, the constraint CDFT calculations with axial symmetric quadrupole (β_2) and octupole (β_3) degrees of freedom are performed within the ranges of $-0.5 \leq \beta_2 \leq 0.6$ and $|\beta_3| \leq 0.4$ with both mesh steps of 0.04. Although the major shell number of the harmonic-oscillator basis $N_f = 16$ is large enough to achieve a convergence of the global minimum binding energy for ^{212}Ra [24], it is found that a large major shell number $N_f = 20$ is necessary to obtain converged solutions for the constraint calculations with large deformation such as $\beta_2 \sim 0.5$. For consistency, $N_f = 20$ is adopted in the present constraint CDFT calculations. For convenience, the results with $\beta_3 = 0$ obtained in the constraint calculations are referred to as “quad” and the results with $\beta_2 = \beta_3 = 0$ are referred to as “sph”. The corresponding lowest minima in the potential energy curves with $\beta_3 = 0$ and the total (β_2, β_3) potential energy surfaces are denoted as $E_{\text{min}}(\beta_2)$ and $E_{\text{min}}(\beta_2, \beta_3)$, respectively.

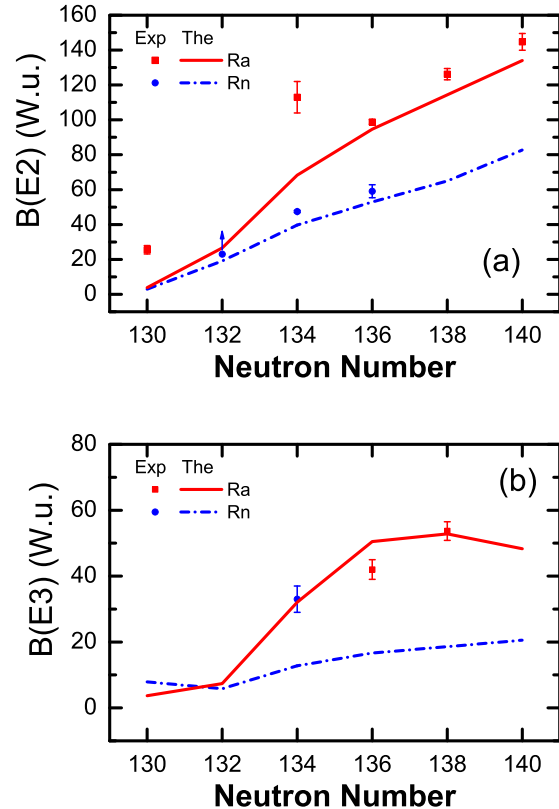
For even-even $^{206-228}\text{Ra}$ and $^{204-226}\text{Rn}$, which are nuclei associated with the δV_{pn} in Ra isotopes with $N = 120-140$, the potential energy surfaces in the (β_2, β_3) plane obtained in the CDFT calculations are shown in Figs. 1 and 2, respectively. The main features and the conclusions drawn in Ref. [24]

FIG. 2. Same as Fig. 1, but for even-even isotopes $^{204-226}\text{Rn}$.

are still held. For the ground states, even-even $^{208-214}\text{Rn}$ and $^{210-216}\text{Ra}$ with $N = 122-128$ are near spherical. With increasing the neutron number away from the magic number $N = 126$, the ground states of the Ra and Rn isotopes become deformed. For $^{216-226}\text{Rn}$ with $N = 130-140$, the ground states are moderately quadrupole deformed with β_3 soft around, except for ^{224}Rn showing an octupole-deformed ground state. For the Ra isotopes, the ground states of $^{218,220}\text{Ra}$ with $N = 130, 132$ are moderately quadrupole deformed and the PESs around display the transitional property to an octupole deformed minimum, whereas the ground states of $^{222-228}\text{Ra}$ with $N = 134-140$ have become octupole deformed with moderate quadrupole deformation. Thus for heavier isotopes $^{222-228}\text{Ra}$, the obtained minima in the calculations with $\beta_3 = 0$ are actually the saddle points in the (β_2, β_3) plane. It is noted that the obtained quadrupole deformations β_2 for the ground states of $^{218,222,224,226,228}\text{Ra}$ and $^{220,222}\text{Rn}$ are 0.058, 0.167, 0.185, 0.204, 0.214 and 0.125, 0.141, respectively, in good agreement with the available empirical values 0.091, 0.192, 0.179, 0.202, 0.217 and 0.127, 0.142 [55]. Similar PESs of ^{224}Ra and ^{220}Rn were obtained in the Hartree-Fock-Bogoliubov theory with Gogny D1M interaction [19]. In a previous reflection asymmetric relativistic study with effective interactions NL3* [56] and PK1 [57], similar pattern of shape evolution in the Ra isotopes was also found in the Th isotopes [58].

Figure 3 displays the calculated $B(E2; 2_1^+ \rightarrow 0_1^+)$, and $B(E3; 3_1^- \rightarrow 0_1^+)$ as functions of the neutron number for Ra and Rn isotopes. In Fig. 3(a), the $B(E2)$ values increase gradually with increasing neutron number and reasonably agree with the available experimental data [55,59,60], showing a clear shape evolution from nearly spherical to well-deformed shapes for both Ra and Rn chains. Similar agreement was obtained by the GCM calculations based on the HFB theory [19]. In Fig. 3(b), the calculated $B(E3)$ of Ra isotopes increases from $N = 130$ to 138, and then decreases with N , which is

consistent with the octupole shape evolution displayed by the PES in Fig. 1. The pronounced $B(E3)$ experimental values of ^{224}Ra and ^{226}Ra can be reasonably reproduced by the QOCH calculations with only a small overestimation for ^{224}Ra . As discussed in Ref. [44], the overestimation is possibly related

FIG. 3. The calculated $B(E2; 2_1^+ \rightarrow 0_1^+)$, and $B(E3; 3_1^- \rightarrow 0_1^+)$ (in units of W.u.) as functions of the neutron number for Ra and Rn isotopes, in comparison with the data available [55,59,60].

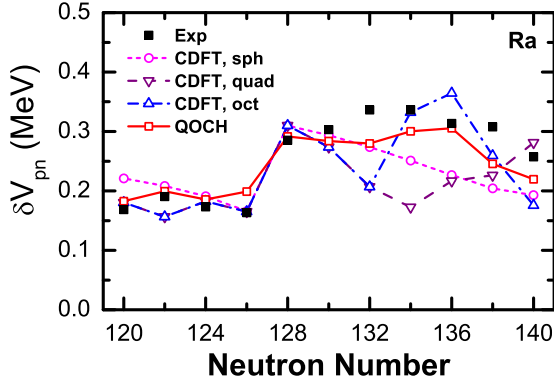


FIG. 4. The δV_{pn} for even-even $^{208-228}\text{Ra}$ obtained in spherical, β_2 -constrained and β_2, β_3 -constrained CDFT with effective interaction PC-PK1, together compared with collective QOCH result and experimental data [63].

to weaker pairing correlations [61] and it was shown that the $B(E3)$ exhibits a marked decrease as pairing strength increases for ^{224}Ra [44]. The calculated $B(E3)$ of Rn isotopes is in general smaller than those of Ra isotopes. For ^{220}Rn , the underestimation of the datum may be because the present model only includes the $K = 0$ components (axial symmetry), and the mixing with $K = 0$ might become important in nearly spherical nuclei [44,62].

The values of δV_{pn} for even-even $^{208-228}\text{Ra}$ isotopes extracted from the total energies by the constraint CDFT calculations as well as those by the QOCH calculations are plotted in Fig. 4, in comparison with the experimental data [63].

It can be seen in Fig. 4 that the experimental δV_{pn} displays small changes ranging 163–191 keV for $N = 120$ –126, then suddenly jumps to 285 keV at $N = 128$. This sudden jump of δV_{pn} can be ascribed to the effect of shell closure $N = 126$. After the jump, a peak with $\delta V_{pn} \sim 336$ keV is formed at $N = 132, 134$ with slow changes on both sides, keeping the value of δV_{pn} in $128 \leq N \leq 140$ larger than 250 keV.

For the theoretical δV_{pn} , one can find the following main features:

- (i) The sph results extracted from the constraint CDFT calculations with $\beta_2 = \beta_3 = 0$ can reproduce the slow decrease from $N = 120$ to $N = 126$ and the sudden jump at $N = 126$ in the experimental data, but give a constant decreasing slope and fail to reproduce the data for $N \geq 128$.
- (ii) The quad results extracted from the minimal energies in the constraint CDFT calculations with $\beta_3 = 0$ improve the agreement with the data for $N = 120$ to $N = 126$ and reproduce the sudden jump at $N = 126$ as well. For $N \geq 128$, the quad results also fail to reproduce the experimental data, although they greatly change the fine structure of the sph results by considering the quadrupole deformation.
- (iii) The oct results given by the constraint CDFT calculations do not change the agreement of the quad results with the data for $N = 120$ to $N = 132$, as the calculated ground states of the Ra and Rn isotones with

$120 \leq N \leq 132$ are actually quadrupole deformed. For $N \geq 134$, however, the oct results greatly change the quad results and present an obvious peak around $N \sim 136$, leading to a reasonable reproduction to the peak of the experimental δV_{pn} .

In Fig. 4, the theoretical curves with deformation constraints reproduce the experimental δV_{pn} in reasonable levels. With spherical constraints, the δV_{pn} in Fig. 4 gives a continuous decreasing slope when $N \geq 128$. The consideration of the static deformation β_2 and β_3 greatly changes the fine structure of the δV_{pn} in Fig. 4. Since the calculated ground states for the isotopes $120 \leq N \leq 132$ are not octupole deformed, the δV_{pn} values extracted from $E_{\min}(\beta_2, \beta_3)$ coincide with those from $E_{\min}(\beta_2)$. Instead of the δV_{pn} from $E_{\min}(\beta_2)$, the δV_{pn} concerning β_3 basically gives good trend from $N = 134$ to $N = 140$. It is shown in Fig. 4 that the introduction of β_3 dramatically changes the δV_{pn} at $N = 134, 136, 140$ for about 150 keV, nearly half of their absolute values. It is further noted that pairing correlation also plays an important role, since in the calculations without pairing [24], δV_{pn} gets large values around 500 keV near $N = 136$, and drops to a negative value at $N = 140$.

With the consideration of β_2 and β_3 in the CDFT, some discrepancies to the experimental data still exist, such as the one at $N = 132$. To investigate the beyond-mean-field effect, the δV_{pn} derived from the QOCH calculations are also presented in Fig. 4. It can be clearly seen that the trend and the quantitative values of δV_{pn} are well reproduced by the QOCH with the consideration of both static deformation and collective fluctuation. Taking the sph results of δV_{pn} in Fig. 4 as a baseline, the modifications by the deformation and fluctuations are opposite for $N = 132, 134, 136$. Both the static deformation and the collective fluctuation play important roles in getting better description on the fine structure of δV_{pn} . Quantitatively, the δV_{pn} for Ra isotopes with $N = 130$ –140 by the QOCH are more close to the empirical value. Given the root-mean-square (rms) energy deviation for the selected 60 spherical nuclei with effective interaction PC-PK1 [39] is 1.33 MeV on average, the accuracy of δV_{pn} is remarkable. In the context of deformed HFB with Gogny energy density functionals and GCM calculations, the δV_{pn} for Ra and Th isotopes have been discussed [19]. It was also found that after considering the octupole degree of freedom and collective correlations, good agreement with experimental δV_{pn} can be obtained. Similar conclusion holds here as the static deformation brings sharp changes to the δV_{pn} while the collective fluctuation smoothly corrects the δV_{pn} with good trend.

For a close look, the calculated ground-state energy $E(0^+)$ obtained by QOCH method can be decomposed into several terms from the static deformation and the collective fluctuation. The energies involved with the static deformation include the quadrupole deformation energy $E_{\text{quad}} = E_{\min}(\beta_2) - E_{\text{sph}}$ and the octupole deformation energy $E_{\text{oct}} = E_{\min}(\beta_2, \beta_3) - E_{\min}(\beta_2)$. The contribution from the collective fluctuation, $E(0^+) - E_{\min}(\beta_2, \beta_3)$, can be further decomposed into three terms: the vibrational and rotational ZPE denoted by ΔV_{vib} and ΔV_{rot} as well as the collective correlation energy E_{corr} defined by $E(0^+) - [E_{\min}(\beta_2, \beta_3) - \Delta V_{\text{vib}} - \Delta V_{\text{rot}}]$.

TABLE I. The energy differences among the experimental binding energies E_{exp} , the binding energies constrained to spherical E_{sph} , the minimum binding energies for the β_2 -constrained states $E_{\text{min}}(\beta_2)$, the binding energies for the ground states in the (β_2, β_3) plane $E_{\text{min}}(\beta_2, \beta_3)$ obtained by CDFT with effective interaction PC-PK1, and the energies of the $I^\pi = 0^+$ ground-state $E(0^+)$ obtained by QOCH method for even-even $^{220,222}\text{Rn}$ and $^{222,224}\text{Ra}$. The vibrational and rotational ZPE denoted by ΔV_{vib} and ΔV_{rot} and E_{corr} defined by $E(0^+) - [E_{\text{min}}(\beta_2, \beta_3) - \Delta V_{\text{vib}} - \Delta V_{\text{rot}}]$ are also listed. The last row lists partial contribution corresponding to each term. The unit of energy is MeV.

nuclei	E_{exp}	E_{sph}	E_{quad}	E_{oct}	$-\Delta V_{\text{vib}}$	$-\Delta V_{\text{rot}}$	E_{corr}	$E(0^+)$
^{220}Rn	-1697.794	-1693.915	-1.761	0.000	-2.102	-1.312	1.625	-1697.465
^{222}Rn	-1708.177	-1703.608	-2.209	0.000	-2.113	-1.466	1.673	-1707.724
^{222}Ra	-1708.664	-1704.914	-1.103	-0.639	-2.290	-1.743	2.047	-1708.641
^{224}Ra	-1720.301	-1715.514	-1.512	-1.230	-2.153	-1.762	2.049	-1720.121
δ	0.314	0.227	-0.010	0.148	-0.059	-0.037	0.034	0.305

Since the δV_{pn} of one nucleus is the double energy difference associated with four nuclei, taking ^{224}Ra as an example, the above decomposition terms of $^{220,222}\text{Rn}$ and $^{222,224}\text{Ra}$ are tabulated in Table I. The nucleus ^{224}Ra was suggested to be octupole deformed based on the measured $E\lambda$ transitions [60] and has been well studied on top of CDFT with the beyond-mean-field approaches [44,64,65]. The data in Table I are visualized in Fig. 5 with a multiply factor of 1/4. There are four parts in this figure, i.e., $E_{\text{sph}} - E_{\text{exp}}$, E_{quad} stacking with E_{oct} , $-\Delta V_{\text{vib}}$ stacking with $-\Delta V_{\text{rot}}$, and E_{corr} . In each part, four columns stand for the corresponding terms of ^{220}Rn , ^{222}Rn , ^{222}Ra , and ^{224}Ra , respectively. Since $\delta V_{pn}(^{224}\text{Ra}) = \frac{1}{4}[-E(^{220}\text{Rn}) + E(^{222}\text{Rn}) + E(^{222}\text{Ra}) - E(^{224}\text{Ra})]$, the contribution from each part to δV_{pn} is the sum of the columns of ^{222}Rn and ^{222}Ra minus those of ^{220}Rn and ^{224}Ra . Following the decomposition scheme, the nesting corrections for $\delta V_{pn}(^{224}\text{Ra})$ can be obtained, as shown in Table I. In detail, the δV_{pn} at $N = 136$ obtained from E_{sph} is 227 keV, 87 keV smaller than the empirical data 314 keV. The quadrupole approximation happens to bring little correction -10 keV to

δV_{pn} , although the quadrupole deformation energies of the four nuclei vary from -1.103 to -2.209 MeV. The most significant correction 148 keV is brought by the consideration of the octupole degree of freedom, which is because E_{oct} changes from -0.639 MeV in ^{222}Ra to -1.230 MeV in ^{224}Ra and no static octupole deformation in the Rn isotones in Table I. For the collective fluctuation, three composing terms $-\Delta V_{\text{vib}}$, $-\Delta V_{\text{rot}}$, and E_{corr} bring -59 keV, -37 keV, and 34 keV corrections to δV_{pn} , in total -62 keV. It is clear that the contribution from the octupole deformation is the most, and the contributions from collective fluctuation are also important. Note the contributions from the static octupole deformation and the collective fluctuation are opposite.

To understand the octupole correlations microscopically, the neutron and proton single-particle levels of ^{224}Ra are shown in Fig. 6 as functions of deformation parameters β_2 and β_3 . For the neutron levels in Fig. 6(a), three levels with low- Ω originating from the $1i_{11/2}$ level and two levels with low- Ω from the $2g_{9/2}$ level go down when the quadrupole deformation increases from zero to the saddle point. When the octupole deformation increases together with the increasing quadrupole deformation from the saddle point to the ground state, one level with the first leading component $\nu 5/2[633]$ from $1i_{11/2}$ goes up whereas another level with the first leading component $\nu 1/2[660]$ from $2g_{9/2}$ goes down more steeply, making an energy gap with $N = 132$ emerge near the ground state. For the proton levels in Fig. 6(b), an energy gap with $Z = 88$ near the Fermi surface is found, that is because one level $\pi 5/2[523]$ from $1g_{9/2}$ goes up and another level $\pi 1/2[550]$ from $2f_{7/2}$ goes down steeply. These two levels $\pi 5/2[523]$ and $\pi 1/2[550]$ behave very similar to the neutron levels $\nu 5/2[633]$ and $\nu 1/2[660]$ just mentioned. Above $N = 132$ and $Z = 88$, energy gaps with $N = 136$ and $Z = 92$ can also be seen in Figs. 6(a) and 6(b), respectively. Thus, it can be inferred that the nucleus with neutron number $N = 132, 134$, or 136 and proton number $Z = 88, 90$, or 92 is more likely to have an octupole-deformed minimum. It is not surprising that the ground states of ^{224}Ra and neighboring nuclei are octupole deformed in the CDFT calculations.

In the CDFT calculation, each single-particle level is decomposed into various components of the harmonic oscillator basis, i.e., $\psi = \sum_i \alpha_i^2 \phi_i$ using Nilsson-like notations $\Omega[N, n_z, m_l]$ for neutron or proton. It is known that one component ϕ_{i1} with the quantum numbers $\Omega[N, n_z, m_l]$ and

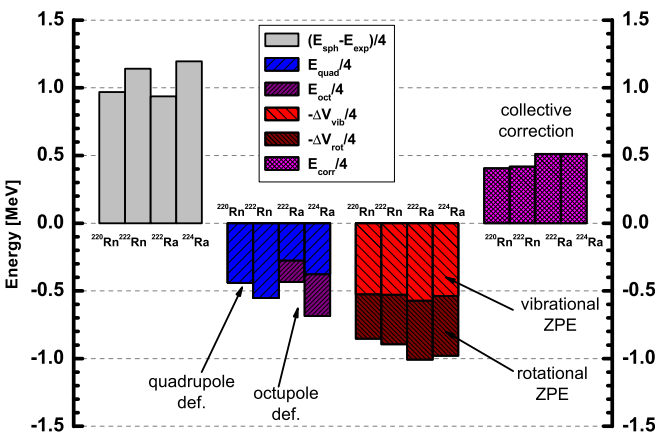


FIG. 5. Contributions from the static deformation and the collective fluctuation for $^{220,222}\text{Rn}$ and $^{222,224}\text{Ra}$. The energies with the static deformation are the quadrupole deformation energy $E_{\text{quad}} = E_{\text{min}}(\beta_2) - E_{\text{sph}}$ the octupole deformation energy $E_{\text{oct}} = E_{\text{min}}(\beta_2, \beta_3) - E_{\text{min}}(\beta_2)$. The contribution terms for the collective fluctuation read the vibrational ZPE ΔV_{vib} , the rotational ZPE ΔV_{rot} and the correction energy $E_{\text{corr}} = E(0^+) - [E_{\text{min}}(\beta_2, \beta_3) - \Delta V_{\text{vib}} - \Delta V_{\text{rot}}]$.

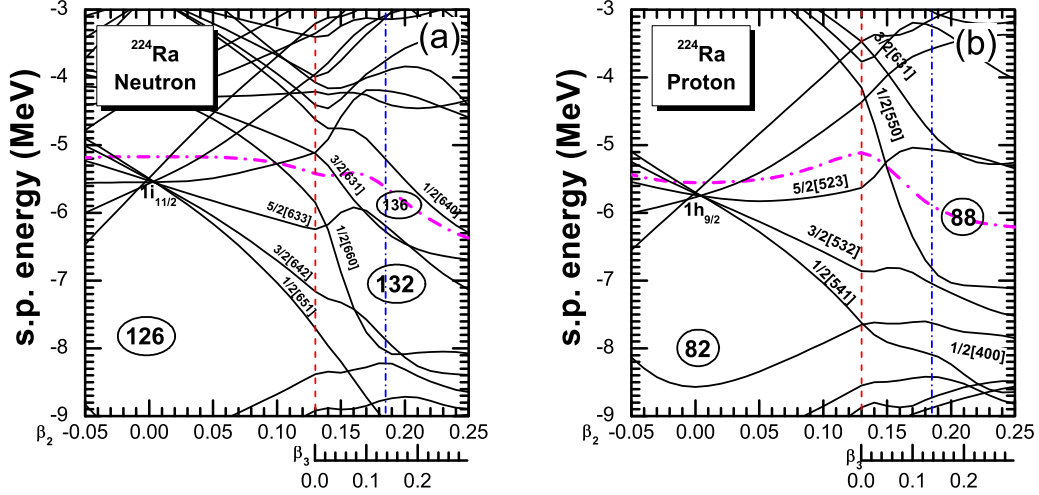


FIG. 6. Neutron (a) and proton (b) single-particle levels of ^{224}Ra in CDFT with PC-PK1 as functions of β_2 . The dash-dot lines denote the corresponding Fermi surfaces. The levels near the Fermi surface are labeled by Nilsson notations $\Omega[Nn_z m_l]$ of the first leading component. The states with $\beta_2 \leq 0.13$ in the left part are purely quadrupole deformed connecting the oblate state and the quadrupole-deformed saddle point, while the states with $\beta_2 > 0.13$ in the right part are quadrupole -octupole deformed connecting the saddle point and the octupole-deformed ground state.

another component ϕ_{i2} with the quantum numbers $\Omega[N + 1, n_z \pm 3, m_l]$ form an octupole driving pair [66]. Therefore the summed octupole component contribution $\sum \alpha_{i1} \alpha_{i2}$ may provide a measurement of octupole driving strength. A study of ^{292}Cm shows that the summed contribution behaves like a switch [38], as it becomes large for quadrupole-octupole deformed state and turns into zero for purely quadrupole-deformed state.

Taking the two single-particle levels $\nu 1/2[660]$ and $\pi 1/2[550]$ as examples, the expansion components of them for the ground state of ^{224}Ra are listed in Table II. For $\nu 1/2[660]$, the first leading component $1/2[660]$ has one octupole partner $1/2[530]$. Four more driving pairs, namely $1/2[631]-1/2[501]$, $1/2[550]-1/2[620]$, $1/2[750]-1/2[880]$, and $1/2[440]-1/2[510]$ can be found in the components that contribute no less than 1%. In total, an considerable summed contribution 0.542 is obtained for this neutron level. For the proton level $\pi 1/2[550]$, the accumulated contribution reaches 0.550. It is noted that there is one component $1/2[640]$ having two driving partners, namely $1/2[770]$ and $1/2[510]$. Other components may also have more than one partners which are not listed here due to small contributions.

In Ref. [7], the proton-neutron interaction is discussed in terms of spatial overlaps of proton and neutron wave functions. It is suggested that nuclear collectivity is driven by synchronized filling of protons and neutrons with orbitals having parallel spins, identical orbital, and total angular momentum projections, belonging to adjacent major shells and differing by one quantum of excitation along the z axis. Explicitly, for a neutron orbital $\Omega[N, n_z, m_l]$, the proton orbital $\Omega[N \pm 1, n_z \pm 1, m_l]$ satisfying $\Delta\Omega[\Delta N, \Delta n_z, \Delta m_l] = 0[110]$ has large spatial overlap with it, and their proton-neutron interaction may be enhanced. Thus in the following part, the components of the neutron and proton single-particle levels near the Fermi surfaces will be cross checked with whether the empirical relation $\Delta\Omega[\Delta N, \Delta n_z, \Delta m_l] = 0[110]$ holds or not.

For the first leading component $1/2[660]$ of the neutron level $\nu 1/2[660]$, as shown in Table II, two components $1/2[550]$ and $1/2[770]$ satisfying the relation $\Delta\Omega[\Delta N, \Delta n_z, \Delta m_l] = 0[110]$ can be found in the proton level $\pi 1/2[550]$. For the second leading component $1/2[631]$ of this neutron level, the component $1/2[521]$ in the proton level satisfies the quantal relation. Among other components in the neutron and proton levels, one can find more such pairs of partners. It is therefore indicated that in ^{224}Ra the

TABLE II. The components of single-particle level $\nu 1/2[660]$ and $\pi 1/2[550]$ at the ground state with $(\beta_2, \beta_3) = (0.185, 0.135)$ in ^{224}Ra , obtained by the constrained CDFT+BCS calculations using PC-PK1 energy density functional. The components contributing no less than 1% are listed for saving space. The octupole driving components $\Omega[N, n_z, m_l]$ and $\Omega[N + 1, n_z \pm 3, m_l]$ are grouped with the same symbols. The summed octupole component contribution (Oct-Sum) is listed at the bottom.

$\nu 1/2[660]$		$\pi 1/2[550]$	
$\diamond 1/2[660]$	21.4%	$1/2[550]$	17.8%
$\triangleleft 1/2[631]$	13.8%	$\ominus 1/2[651]$	16.2%
$\triangleright 1/2[550]$	13.5%	$1/2[530]$	15.2%
$1/2[651]$	11.6%	$\otimes 1/2[631]$	10.7%
$\oplus 1/2[750]$	5.5%	$\circ \bullet 1/2[640]$	7.9%
$\oplus 1/2[880]$	5.0%	$\ominus 1/2[521]$	6.1%
$1/2[770]$	4.2%	$\circ 1/2[510]$	4.5%
$\triangleleft 1/2[501]$	3.6%	$1/2[620]$	3.6%
$\diamond 1/2[530]$	2.0%	$1/2[330]$	1.8%
$\triangleright 1/2[620]$	2.0%	$\bullet 1/2[770]$	1.6%
$1/2[990]$	1.8%	$1/2[431]$	1.0%
$1/2[611]$	1.8%	$1/2[611]$	1.0%
$\odot 1/2[440]$	1.5%	$\otimes 1/2[761]$	1.0%
$\odot 1/2[510]$	1.3%		
Oct-Sum	0.542	Oct-Sum	0.550

synchronized filling of orbitals $\nu 1/2[660]$ and $\pi 1/2[550]$ will enhance the proton-neutron interaction.

Like the example of enhanced proton-neutron interaction in Table II, more instances can be found in the levels near Fermi surface for the octupole deformed states of ^{224}Ra . The neutron level $\nu 1/2[660]$ has significant overlap with the proton levels $\pi 1/2[541]$, $\pi 1/2[530]$, and $\pi 1/2[550]$ while the proton level $\pi 1/2[550]$ has significant overlap with the neutron levels $\nu 1/2[660]$, $\nu 1/2[640]$, and $\nu 1/2[631]$.

IV. CONCLUSION

In summary, the δV_{pn} for even-even Ra isotopes are analyzed in the covariant density functional theory and the quadrupole-octupole collective Hamiltonian model. It is shown that the successive introduction of static deformation and collective fluctuation are crucial ingredients for reproduction of the data. Particularly, the introduction of octupole deformation dramatically changes the δV_{pn} at $N = 134, 136, 140$. The collective fluctuation smoothly corrects the δV_{pn} with good trend. A detailed analysis on the δV_{pn} of ^{224}Ra has been made by decomposing this quantity into

several terms from the static deformation and the collective fluctuation. The contributions are further decomposed and analyzed. For ^{224}Ra , the neutron and proton single-particle levels as functions of deformation are investigated, and by analyzing the components of the wave functions, the octupole driving pairs and the enhancement of proton-neutron interaction are discussed. It is found that the proton-neutron interaction is enhanced as the empirical relation $\Delta\Omega[\Delta N, \Delta n_z, \Delta m_l] = 0[110]$ holds between the neutron levels and proton levels with significant octupole components in ^{224}Ra .

ACKNOWLEDGMENTS

The authors sincerely express the gratitude to Z. P. Li for helpful discussions. This work was supported in part by National Natural Science Foundation of China under Grants No. 11505157, No. 11875075, and No. 11935003, the National Key R&D Program of China (Contract No. 2017YFE0116700), and Physics Research and Development Program of Zhengzhou University (Grant No. 32410217). The theoretical calculation was carried out by the nuclear data storage system in Zhengzhou University.

-
- [1] J. D. Garrett and Z.-Y. Zhang, International Conference on Contemporary Topics in Nuclear Structure Physics, Cocoyoc, Mexico, June, 1988.
- [2] J.-Y. Zhang, R. F. Casten, and D. S. Brenner, *Phys. Lett. B* **227**, 1 (1989).
- [3] P. Van Isacker, D. D. Warner, and D. S. Brenner, *Phys. Rev. Lett.* **74**, 4607 (1995).
- [4] W. Satuła, D. J. Dean, J. Gary, S. Mizutori, and W. Nazarewicz, *Phys. Lett. B* **407**, 103 (1997).
- [5] R. B. Cakirli, D. S. Brenner, R. F. Casten, and E. A. Millman, *Phys. Rev. Lett.* **94**, 092501 (2005).
- [6] R. B. Cakirli and R. F. Casten, *Phys. Rev. Lett.* **96**, 132501 (2006).
- [7] D. Bonatsos, S. Karampagia, R. B. Cakirli, R. F. Casten, K. Blaum, and L. A. Susam, *Phys. Rev. C* **88**, 054309 (2013).
- [8] M. K. Basu and D. Banerjee, *Phys. Rev. C* **3**, 992 (1971); **4**, 652 (1971).
- [9] J. Jänecke, *Phys. Rev. C* **6**, 467 (1972).
- [10] Z. C. Gao and Y. S. Chen, *Phys. Rev. C* **59**, 735 (1999).
- [11] W. A. Friedman and G. F. Bertsch, *Phys. Rev. C* **76**, 057301 (2007).
- [12] G. J. Fu, H. Jiang, Y. M. Zhao, and A. Arima, *Phys. Rev. C* **82**, 014307 (2010).
- [13] G. J. Fu, M. Bao, Z. He, H. Jiang, Y. M. Zhao, and A. Arima, *Phys. Rev. C* **86**, 054303 (2012).
- [14] G. J. Fu, J. J. Shen, Y. M. Zhao, and A. Arima, *Phys. Rev. C* **87**, 044309 (2013).
- [15] Z. Wu, S. A. Changizi, and C. Qi, *Phys. Rev. C* **93**, 034334 (2016).
- [16] M. Stoitsov, R. B. Cakirli, R. F. Casten, W. Nazarewicz, and W. Satuła, *Phys. Rev. Lett.* **98**, 132502 (2007).
- [17] M. Bender and P.-H. Heenen, *Phys. Rev. C* **83**, 064319 (2011).
- [18] C. Qi, *Phys. Lett. B* **717**, 436 (2012).
- [19] L. M. Robledo and P. A. Butler, *Phys. Rev. C* **88**, 051302(R) (2013).
- [20] R. F. Casten and R. B. Cakirli, *Phys. Scr.* **91**, 033004 (2016).
- [21] G. J. Fu, Y. Lei, H. Jiang, Y. M. Zhao, B. Sun, and A. Arima, *Phys. Rev. C* **84**, 034311 (2011).
- [22] D. S. Brenner, R. B. Cakirli, and R. F. Casten, *Phys. Rev. C* **73**, 034315 (2006).
- [23] D. Neidherr, G. Audi, D. Beck, K. Blaum, C. Bohm, M. Breitenfeldt, R. B. Cakirli, R. F. Casten, S. George *et al.*, *Phys. Rev. Lett.* **102**, 112501 (2009).
- [24] L. F. Yu, P. W. Zhao, S. Q. Zhang, and J. Meng, [arXiv:1211.0601](https://arxiv.org/abs/1211.0601) [nucl-th].
- [25] P. A. Butler and W. Nazarewicz, *Rev. Mod. Phys.* **68**, 349 (1996).
- [26] P. Ring, *Prog. Part. Nucl. Phys.* **37**, 193 (1996).
- [27] M. Bender, P.-H. Heenen, and P. G. Reinhard, *Rev. Mod. Phys.* **75**, 121 (2003).
- [28] D. Vretenar, A. V. Afanasjev, G. A. Lalazissis, and P. Ring, *Phys. Rep.* **409**, 101 (2005).
- [29] J. Meng, H. Toki, S.-G. Zhou, S. Q. Zhang, W. H. Long, and L. S. Geng, *Prog. Part. Nucl. Phys.* **57**, 470 (2006).
- [30] J. Meng (Ed.), *Relativistic Density Functional for Nuclear Structure*, International Review of Nuclear Physics Vol. 10 (World Scientific, Singapore, 2016).
- [31] P.-H. Heenen, A. Valor, M. Bender, P. Bonche, and H. Flocard, *Eur. Phys. J. A* **11**, 393 (2001).
- [32] R. Rodriguez-Guzman, L. M. Robledo, and P. Sarriguren, *Phys. Rev. C* **86**, 034336 (2012).
- [33] W. Zhang, Z. P. Li, and S. Q. Zhang, *Phys. Rev. C* **88**, 054324 (2013).
- [34] T. T. Sun, E. Hiyama, H. Sagawa, H.-J. Schulze, and J. Meng, *Phys. Rev. C* **94**, 064319 (2016).
- [35] S.-H. Ren, T.-T. Sun, and W. Zhang, *Phys. Rev. C* **95**, 054318 (2017).
- [36] Z.-X. Liu, C.-J. Xia, W.-L. Lu, Y.-X. Li, J. N. Hu, and T.-T. Sun, *Phys. Rev. C* **98**, 024316 (2018).

- [37] W. Zhang and Y. F. Niu, *Phys. Rev. C* **96**, 054308 (2017).
- [38] W. Zhang and Y. F. Niu, *Phys. Rev. C* **97**, 054302 (2018).
- [39] P. W. Zhao, Z. P. Li, J. M. Yao, and J. Meng, *Phys. Rev. C* **82**, 054319 (2010).
- [40] P. W. Zhao, L. S. Song, B. Sun, H. Geissel, and J. Meng, *Phys. Rev. C* **86**, 064324 (2012).
- [41] K. Q. Lu, Z. X. Li, Z. P. Li, J. M. Yao, and J. Meng, *Phys. Rev. C* **91**, 027304 (2015).
- [42] Z. P. Li, B. Y. Song, J. M. Yao, D. Vretenar, and J. Meng, *Phys. Lett. B* **726**, 866 (2013).
- [43] Z. P. Li, T. Nikšić, and D. Vretenar, *J. Phys. G: Nucl. Part. Phys.* **43**, 024005 (2016).
- [44] S. Y. Xia, H. Tao, Y. Lu, Z. P. Li, T. Nikšić, and D. Vretenar, *Phys. Rev. C* **96**, 054303 (2017).
- [45] P. W. Zhao and Z. P. Li, *Int. J. Mod. Phys. E* **27**, 1830007 (2018).
- [46] B. A. Nikolaus, T. Hoch, and D. G. Madland, *Phys. Rev. C* **46**, 1757 (1992).
- [47] T. Bürvenich, D. G. Madland, J. A. Maruhn, and P.-G. Reinhard, *Phys. Rev. C* **65**, 044308 (2002).
- [48] P. Ring and P. Schuck, *The Nuclear Many-Body Problem* (Springer, New York, 1980).
- [49] M. Girod and B. Grammaticos, *Nucl. Phys. A* **330**, 40 (1979).
- [50] D. R. Inglis, *Phys. Rev.* **103**, 1786 (1956).
- [51] S. T. Belyaev, *Nucl. Phys.* **24**, 322 (1961).
- [52] T. Nikšić, Z. P. Li, D. Vretenar, L. Próchniak, J. Meng, and P. Ring, *Phys. Rev. C* **79**, 034303 (2009).
- [53] S. J. Krieger, P. Bonche, H. Flocard, P. Quentin, and M. S. Weiss, *Nucl. Phys. A* **517**, 275 (1990).
- [54] M. Bender, K. Rutz, P.-G. Reinhard, and J. A. Maruhn, *Eur. Phys. J. A* **8**, 59 (2000).
- [55] B. Pritychenko, M. Birch, B. Singh, and M. Horoi, *At. Data Nucl. Data Tables* **107**, 1 (2016).
- [56] G. A. Lalazissis, S. Karatzikos, R. Fossion, D. Pena Arteaga, A. V. Afanasjev, and P. Ring, *Phys. Lett. B* **671**, 36 (2009).
- [57] W. Long, J. Meng, N. Van Giai, and S. G. Zhou, *Phys. Rev. C* **69**, 034319 (2004).
- [58] J. Y. Guo, P. Jiao, and X.-Z. Fang, *Phys. Rev. C* **82**, 047301 (2010).
- [59] T. Kibédi and R. H. Spear, *At. Data Nucl. Data Tables* **80**, 35 (2002).
- [60] L. P. Gaffney *et al.*, *Nature (London)* **497**, 199 (2013).
- [61] S. E. Agbemava, A. V. Afanasjev, and P. Ring, *Phys. Rev. C* **93**, 044304 (2016).
- [62] L. M. Robledo and G. F. Bertsch, *Phys. Rev. C* **84**, 054302 (2011).
- [63] M. Wang, G. Audi, F. G. Kondev, W. J. Huang, S. Naimi, and X. Xu, *Chin. Phys. C* **41**, 030003 (2017).
- [64] J. M. Yao, E. F. Zhou, and Z. P. Li, *Phys. Rev. C* **92**, 041304(R) (2015).
- [65] Y. Fu, H. Wang, L.-J. Wang, and J. M. Yao, *Phys. Rev. C* **97**, 024338 (2018).
- [66] W. Nazarewicz, in *Nuclear Shapes and Nuclear Structure at Low Excitation Energies*, edited by M. Vergnes *et al.* (Plenum Press, New York, 1992), p. 258.